Supporting Information

Delayed hepatic uptake of multi-phosphonic acid poly(ethylene glycol) coated iron oxide measured by real-time Magnetic Resonance Imaging

G. Ramniceanu[1], B.-T. Doan[1], C. Vezignol[2], A. Graillot[3], C. Loubat[3], N. Mignet[1] and J.-F. Berret[2]

[1]Unité de pharmacologie Chimique génétique et d'imagerie, UMR8151/INSERM U1022 CNRS, 4 avenue de l'Observatoire, 75006 Paris, France.
[2]Matière et Systèmes Complexes, UMR 7057 CNRS Université Denis Diderot Paris-VII, Bâtiment Condorcet, 10 rue Alice Domon et Léonie Duquet, 75205 Paris, France.
[3]Specific Polymers, ZAC Via Domitia, 150 Avenue des Cocardières, 34160 Castries, France

Outline

Additional Supporting Information

Movies

Movie representing the image sequence of the liver for mice being treated with PAA_{2K} coated particles (left) and with multi-phosphonic acid PEG_{2K} coated particles (right), both being 6.8 nm in magnetic core diameter. The movie is made of 29 images taken for 100 minutes after intravenous injection.

S1 – Characterization of iron oxide nanoparticles: Transmission electron microscopy (TEM)

TEM was carried out on a Jeol-100 CX microscope at the SIARE facility of University Pierre et Marie Curie (Paris 6). TEM was used to characterize the individual nanoparticles. Fig. S1a displays the example of γ-Fe_2O_3 nanoparticles at the magnification of 160000×. The data were fitted by a log-normal function of diameter D_0^{TEM} and size dispersity s^{TEM}.

$$p\left(D,D_0^{TEM},s^{TEM}\right)=\frac{1}{\sqrt{2\pi}\beta(s^{TEM})D}exp\left(-\frac{ln^2(D/D_0^{TEM})}{2\beta(s^{TEM})^2}\right)$$

In the previous equation, $\beta(s^{TEM})$ is related to the particles size dispersity s^{TEM} by the relationship $\beta(s^{TEM})=\sqrt{ln(1+s^{TEM2})}$. The size and size dispersity of the different batches studied here are listed in Tab. II (main text).

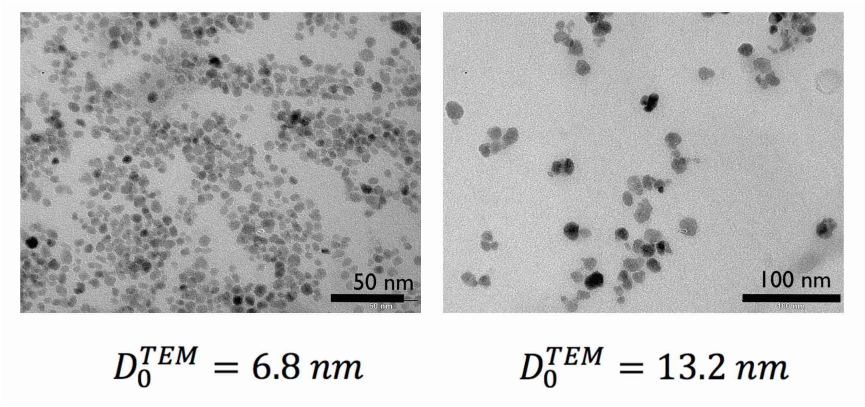

Figure S1a*: Images of transmission electron microscopy of iron oxide nanoparticles.*

The number-averaged molecular weight of the nanoparticles, M_n^{Part} was obtained by dividing the weight-averaged molecular weight M_w^{Part} by the molar-mass dispersity Đ. The Đ's of the polymers was estimated from the size distribution found with TEM. Fig. S1b shows the evolution of $Đ(s)$ assuming a long-normal distribution for the size. As expected, uniform colloids are characterized by $s=0$ and $Đ=1$. With this correspondence, we found that the 6.8 nm and 13.2 nm particles have molar-mass dispersity of 1.43 and 1.61 respectively.

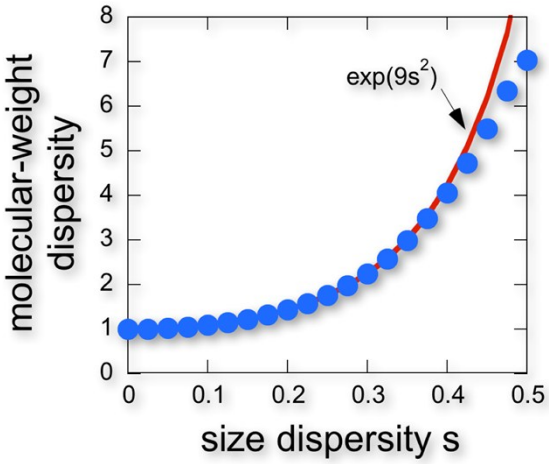

***Figure S1b**: Correspondence between the molecular-weight dispersity (Đ) as defined for polymers, and the size dispersity (s) as defined for colloids.*

S2 – Characterization of iron oxide nanoparticles: Electron beam microdiffraction

Electron beam microdiffraction experiments were performed on the iron oxide dispersion using a Jeol-100 CX transmission electron microscope at the SIARE facility of University Pierre et Marie Curie (Université Paris 6). The electron beam was focused on a selected area comprising a large number of nanoparticles, which diffraction pattern was recorded in the Fourier plane of the microscope (Fig. S2). The reinforcement of the scattering along the rings is interpreted as arising from the diffraction by nanoparticles of different orientations with respect to the incoming beam. The wave-vector dependence of the intensity is shown in Fig. S2. The high crystallinity of the nanoparticles was evidenced by the observation of Bragg reflections that were indexed thanks to a calibration with gold and attributed to maghemite iron oxide (γ-Fe_2O_3).

Table S2 provides the list of the Bragg wave-vectors and Miller indices for γ-Fe_2O_3. The positions of the Bragg peaks found experimentally for maghemite nanoparticles compare well with those predicted for this structure.

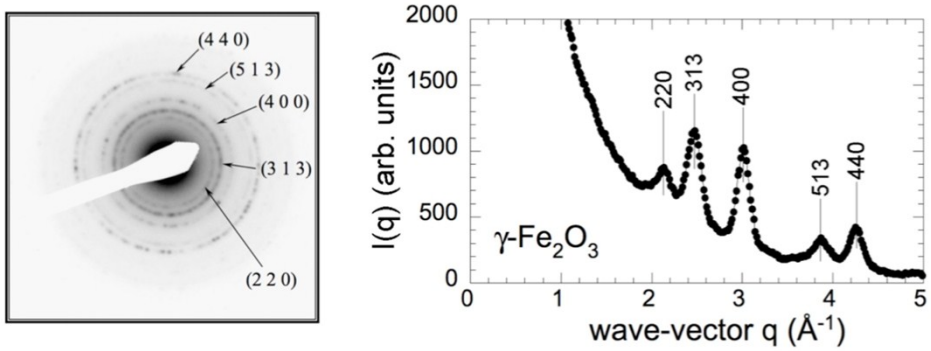

Figure S2*: Microdiffraction spectrum obtained for iron oxide nanoparticles (left). Wave-vector dependence of the scattering intensity obtained for iron oxide nanoparticles (right).*

Theoretical values and proportions for γ-Fe_2O_3			**Experimental data**
Miller indices for maghemite structure	q_i (Å^{-1})	Proportions	q_i (Å^{-1})
(2 2 0)	2.1299	30 %	2.13
(3 1 3)	2.5033	100 %	2.47
(4 0 0)	3.0063	15 %	3.01
(4 2 6)	3.6960	9 %	n.d
(5 1 3)	3.9270	20 %	3.86
(4 4 0)	4.2743	40 %	4.26

Table S2*: Theoretical Miller indices, Bragg wave-vectors and proportions for maghemite structure, and experimental wave-vectors for the peaks observed in Fig. S2. The theoretical data are from R.M. Cornell, U. Schwertmann, 1996, The iron oxides structure, properties, reactions, occurrences and uses, V.C.H., Weinheim.*

S3 – Characterization of iron oxide nanoparticles: Vibrating sample magnetometry (VSM)

Vibrating sample magnetometry (VSM) consisted in measuring the magnetization versus excitation M(H) for a solution at volume fraction φ from the signal induced in detection coils when the sample is moved periodically in an applied magnetic field. Here we used the superparamagnetic nanoparticles having dominant populations at 6.7 and 10.7 nm. Fig. S3 shows the evolution of the macroscopic magnetization M(H) normalized by its saturation value M_S for the γ–Fe_2O_3 superparamagnetic nanoparticles. Here, $M_S = \varphi m_S$, where m_S is the specific magnetization of colloidal maghemite ($m_S = 3.5\times10^5$ A m^{-1}) and ϕ the volume fraction. The solid line in Fig. S3 was obtained using the Langevin function for superparamagnetism convoluted with a log-normal distribution function of the particle size. The parameters of the distribution are the median diameter D_0^{VSM} and the size dispersity s^{VSM}. These values are in relative good agreement with the ones obtained by TEM, albeit from a minor difference in diameter which could originate from defects located close to the surface and that would not contribute to magnetic properties.

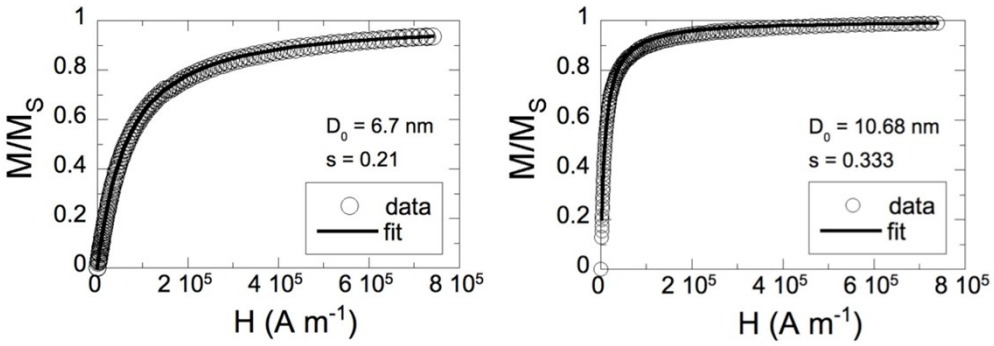

Figure S3: *Magnetic field dependence of the macroscopic magnetization M(H) normalized by its saturation value M_S for cationic maghemite dispersions. The solid curve was obtained using the Langevin equation convoluted with a log-normal distribution of particle sizes.*

S4– Electrophoretic mobility and zeta potential

ζ-potential and electrophoretic mobility μ_E measurements were performed using a Zetasizer NanoZS (Malvern Instrument). Using laser Doppler velocimetry, the technique is based on the Phase Analysis Light Scattering (PALS) method. The data for the two quantities are listed in Table S4 and show that citrate and PAA_{2K}-coated particles were negatively charged, and that PEG-coated particles are neutral.

nanoparticles	zeta potential ζ (mV)	electrophoretic mobility μ_E (10^{-4} cm^2 V^{-1})
citrate γ-Fe_2O_3 (6.8 nm)	- 43	- 3.35
PAA_{2K} γ-Fe_2O_3 (6.8 nm)	- 48	- 3.76
PEG phosphonic acid γ-Fe_2O_3 (6.8 nm)	-5.4	-0.42
PEG phosphonic acid γ-Fe_2O_3 (13.2 nm)	-6.5	-0.51

Table S4 *: Zeta potential (ζ) and electrophoretic mobility (μ_E) for coated iron oxide particles.*

S5 – Determination of the PEG density at the particle surface

As mentioned in the main text and in V. Torrisi *et al.* [*Biomacromolecules* ***15****, 3171 (2014)*], the number of adsorbed polymers and the PEG density at the particle surface can be evaluated from the stability diagram of the mixed polymer/particle dispersions. By plotting the hydrodynamic diameter D_H against the mixing ratio X at pH 8 (the mixing being made at pH 2), a transition is found at the critical value noted X_C. The boundary represented by X_C separates two different dispersion states, a state of individually coated particles at low X and a state of micron-sized aggregates and high X. Fig. S5 displays the hydrodynamic diameter of the scattering objects as a function of the mixing ratio X for the two particles and the two phosphonic acid PEG copolymers (PEG_{2K} and PEG_{5K}). For the 6.8 nm particles, the critical X is equal to 1.3 and 0.5 for the PEG_{2K} and PEG_{5K} respectively, whereas it is equals to 5.0 and 2.0 for the 13.2 nm particles.

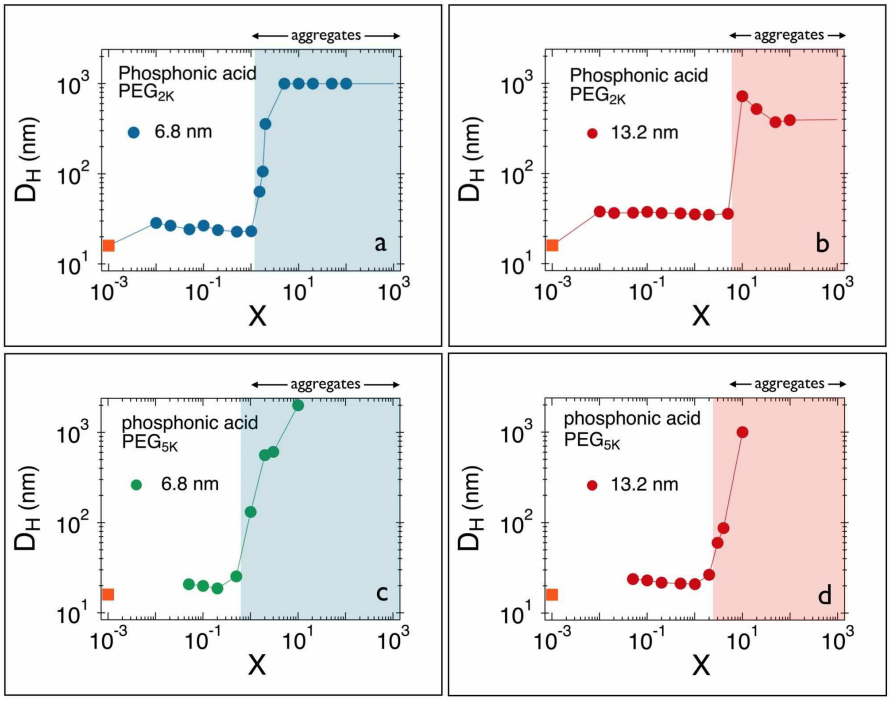

Figure S5: *Stability diagram of mixed γ-Fe_2O_3/polymers dispersions at $pH8$ as a function of the mixing ratio X. X is defined as the ratio between the volumes of nanoparticle and polymer dispersions: a, b) phosphonic acid PEG copolymers with 6.8 nm particles and, c,d) phosphonic acid PEG copolymers with 13.2 nm particles. Above a critical ratio X_C (delimited by the colored area), dispersions are turbid and the particles agglomerate. For micron-sized aggregates, D_H is set at 1 µm for the sake of simplicity. The X_C are given in Table S5.*

As shown previously, the polymer adsorption results from a non-stoichiometric electrostatic binding process which obeys the following rules: below X_C, the iron oxide surfaces are saturated with polymers,

the functional end-groups exceeding the number of binding sites. Above, the coverage is incomplete and the particles precipitate upon pH increase. The number of adsorbed chains per particle n_{ads} is given by:

$$n_{ads} = \frac{1}{X_C} \frac{M_n^{Part}}{M_n^{Pol}}$$

where M_n^{Part} and M_n^{Pol} are the number-average molecular weights of the particle and polymer, respectively. Table S5 provides the list of the polymers and particles characteristics, including thye density of adsorbed polymers n_{ads} and the number of PEG chains per nm^2. We found that the polymers density is twice larger for the 6.8 nm particles (around 2 PEG per nm^2) as for the 13.2 nm, a result that could be due to curvature effects at the particle surface scale.

γ-Fe_2O_3	poly-mers	M_w^{Pol} $g\ mol^{-1}$	M_n^{Pol} $g\ mol^{-1}$	M_w^{Part} $g\ mol^{-1}$	M_n^{Part} $g\ mol^{-1}$	X_C	n_{ads}	PEG per nm^2
6.8 nm	PEG_{2K}	12950	7200	1.3×10^6	9.1×10^5	1.3	97	1.9
	PEG_{5K}	76650	42580	1.3×10^6	9.1×10^5	0.5	43	2.0
13.2 nm	PEG_{2K}	12950	7200	1.2×10^7	7.5×10^6	5.0	207	1.1
	PEG_{5K}	76650	42580	1.2×10^7	7.5×10^6	2.0	88	1.1

***Table S5**: List of the polymer and particles characteristics allowing the calculation of the number of PEG chain per surface unit on the 6.8 and 13.2 nm particles.*

S6 – Nanoparticle distribution kinetics in abdominal aorta monitored by MRI

To follow the distribution of the nanoparticles in the blood, coronal images at the level of the kidneys were also acquired (Fig. S6a and S6b), where the abdominal aorta is clearly visible (white arrow in the upper images a and b). Ranges Of Interest (ROIs) were selected on the blood vessel to monitor the change of signal through time indicating the arrival and then release of the contrast agent in and from the blood circulation. Fig. S6c describes the enhancement of signal as a function of the time for the PEGylated 6.8 nm particles. The data show a 15 % immediate drop of the signal intensity after injection, indicating the presence of the contrast agent in the blood vessel. It is followed by a slow but steady increase of the signal, suggesting that the nanoparticles are filtered out of the blood circuit. The continuous line in green (Fig. S6c) is obtained using a stretched exponential of the form:

$$F_{MRI}(t) = 1 - \alpha \, exp\left[- \left(\frac{t}{\tau}\right)^{\delta} \right]$$

where α = 0.25, τ = 150 min and δ = 2. The relaxation time and stretched exponent are in relative agreement with those obtained from the hepatic uptake for the same contrast agent, confirming that the blood and hepatic signals are inversely related.

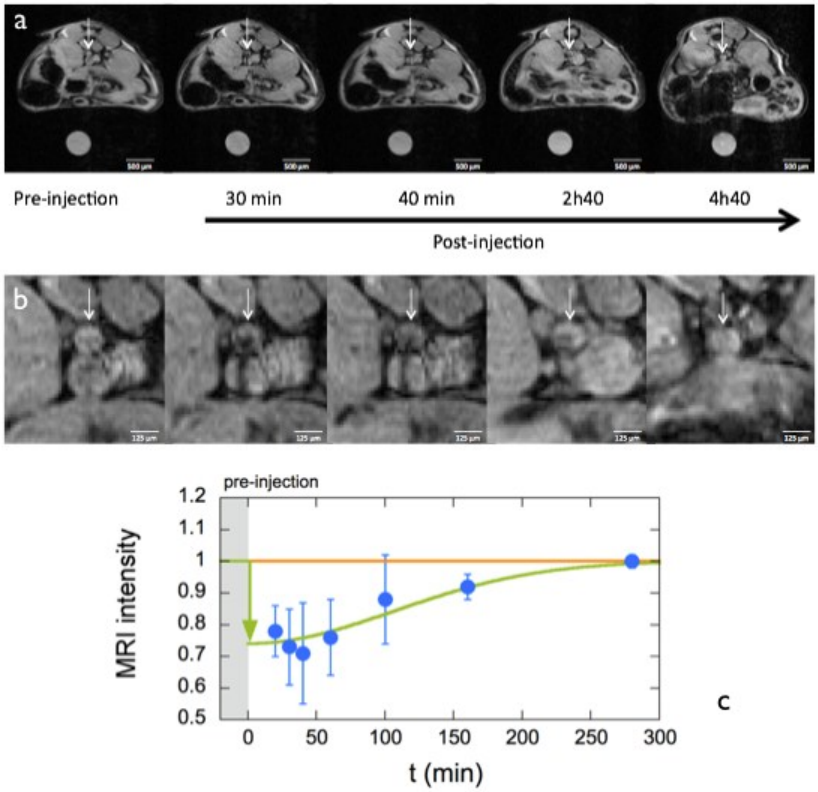

***Figure S6** : a,b) Coronal images of the abdominal aorta at the level of the kidneys prior and after injection of 6.8 nm PEGylated iron oxide. c) Quantification of the MRI signal intensity in the abdominal aorta together with a temporal adjustment using a stretched exponential function.*

S7 – Measurements of the longitudinal and transverse relaxivities in DI-water and in cell culture medium

The longitudinal and transverse relaxivities r_1 and r_2 of the bare and coated particles in DI-water and in cell culture medium were measured using T_1- and T_2-weighted MR images on a 7.0 T on a 300 MHz micro-imaging Bruker spectrometer. Weighted phantom images of dispersions at molar concentration $[Fe]$ = 0, 0.02, 0.05, 0.1, 0.2 and 0.5 mM were acquired. The values of the relaxivities $r_{1,2}$ and relaxivity ratios r_2/r_1 are listed in Table S7 below. Data for r_2 are shown in Fig. 3 of the main text.

		water			cell culture medium		
	coating	r1 $mM^{-1}\,s^{-1}$	r2 $mM^{-1}\,s^{-1}$	r2/r1	r1 $mM^{-1}\,s^{-1}$	r2 $mM^{-1}\,s^{-1}$	r2/r1
γ-Fe_2O_3 6.8 nm	bare	3.3	62	19	1.4	284	197
	citrate	4.0	98	24	nd	nd	nd
	PAA2K	2.7	79	29	1.7	93	55
	PEG2K	1.9	74	39	1.6	77	48
	PEG5K	3.2	118	37	2.7	101	37
γ-Fe_2O_3 13.2 nm	bare	1.6	171	107	0.8	272	340
	citrate	1.4	210	150	1.2	188	157
	PAA2K	1.4	272	197	1.1	281	255
	PEG2K	0.8	226	282	0.6	233	222
	PEG5K	1.8	274	152	1.1	233	211
cliavist©	dextran	3.4	368	108	nd	nd	nd

Table S7: *List of the relaxivities measured for the bare and coated particles studied in this work. Data for r_2 are shown in Fig. 3 of the main text.*

S8 – Cytotoxicity studies using murine hepatocyte BWTG3 and WST-1 assays

The viability of murine hepatocyte cells BWTG3 was studied using WST-1 assay at iron dose levels between 10^{-3} mM to 10 mM. Fig. S8 a-f display the percentage of viable BWTG3 cells treated during 24 h with Cliavist® and with the 6.8 nm and 13.2 nm iron oxides.

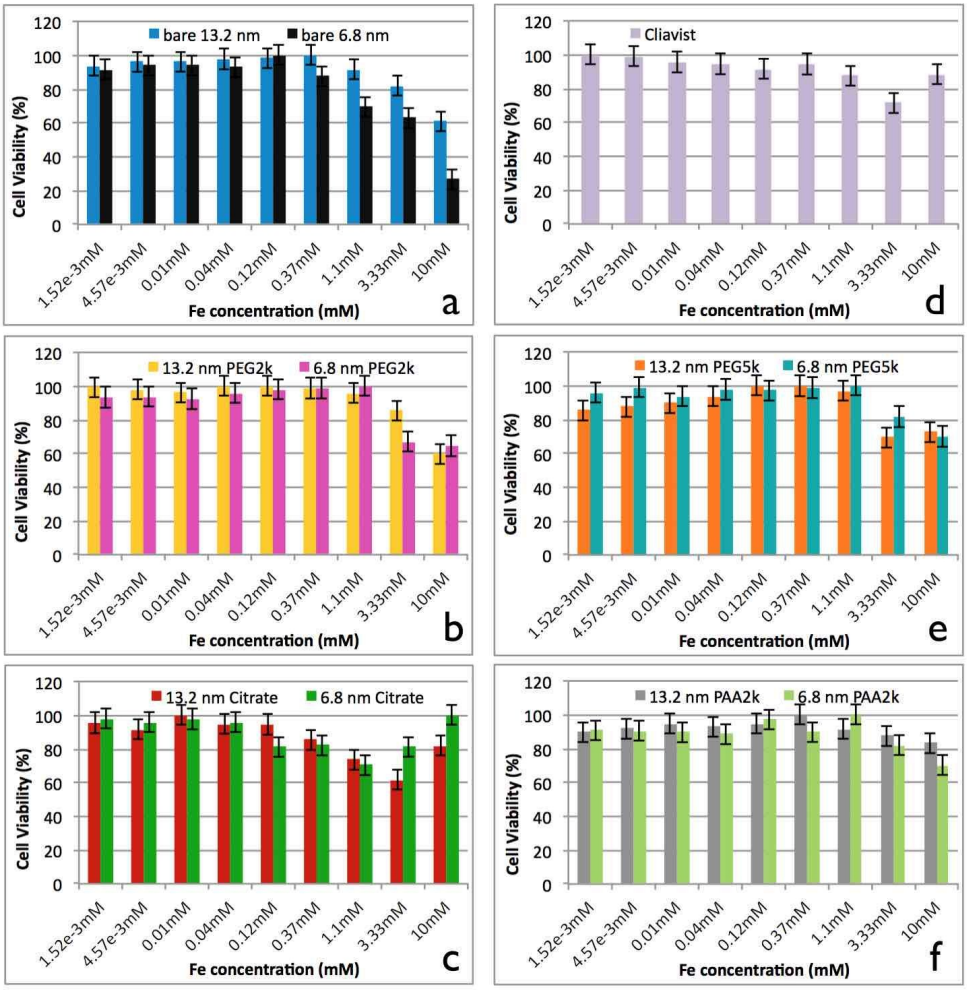

***Figure S8**: Cell viability of murine hepatocyte cells BWTG3 treated with bare and coated iron oxide particles. a) bare; b) phosphonic acid PEG_{2K} copolymers; c) citrate; d) Cliavist®; e) phosphonic acid PEG_{5K} copolymers; f) poly(acrylic acid) 2000 g mol^{-1}.*